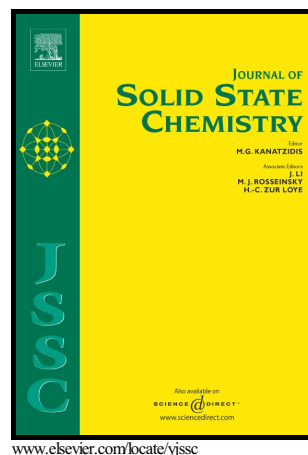


Author's Accepted Manuscript

Al-doped TiO₂ mesoporous material supported Pd with enhanced catalytic activity for complete oxidation of ethanol

Jing Zhu, Wentao Mu, Liqing Su, Xingying Li, Yuyu Guo, Shen Zhang, Zhe Li



PII: S0022-4596(17)30036-1
DOI: <http://dx.doi.org/10.1016/j.jssc.2017.01.028>
Reference: YJSSC19676

To appear in: *Journal of Solid State Chemistry*

Received date: 23 November 2016
Revised date: 19 January 2017
Accepted date: 30 January 2017

Cite this article as: Jing Zhu, Wentao Mu, Liqing Su, Xingying Li, Yuyu Guo, Shen Zhang and Zhe Li, Al-doped TiO₂ mesoporous material supported Pd with enhanced catalytic activity for complete oxidation of ethanol, *Journal of Solid State Chemistry*, <http://dx.doi.org/10.1016/j.jssc.2017.01.028>

This is a PDF file of an unedited manuscript that has been accepted for publication. As a service to our customers we are providing this early version of the manuscript. The manuscript will undergo copyediting, typesetting, and review of the resulting galley proof before it is published in its final citable form. Please note that during the production process errors may be discovered which could affect the content, and all legal disclaimers that apply to the journal pertain

Al-doped TiO₂ mesoporous material supported Pd with enhanced catalytic activity for complete oxidation of ethanol

Jing Zhu, Wentao Mu, Liqing Su, Xingying Li, Yuyu Guo, Shen Zhang, Zhe Li*

College of Chemistry and Chemical Engineering, Taiyuan University of Technology, Taiyuan 030024, Shanxi, China

mlczjsls123@163.com

mwt15035687833@163.com

suliqing0163@163.com

lixingying0479@link.tyut.edu.cn

guoyuyu0455@link.tyut.edu.cn

zhangshen0472@link.tyut.edu.cn

lizhe@tyut.edu.cn

*Corresponding author. Tel./fax: +86 03516018975.

Abstract

Pd catalysts supported on Al-doped TiO₂ mesoporous materials were evaluated in complete oxidation of ethanol. The catalysts synthesized by wet impregnation based on evaporation-induced self-assembly were characterized by X-ray diffraction, measurement of pore structure, XPS, FT-IR, temperature programmed reduction and TEM. Characteristic results showed that the aluminium was doped into the lattice of mesoporous anatase TiO₂ to form Al-O-Ti defect structure. Catalytic results revealed that Al-doped catalysts were much more active than the pristine one, especially at low temperature (≤ 200 °C). This should be ascribed to the introduction of aluminium ions that suppressed the strong metal-support interaction and increased the active sites of Pd oxides, enhanced the stabilized anatase TiO₂, improved well dispersed high valence palladium species with high reducibility and enriched chemisorption oxygen.

graphical abstract

Al-doped Pd/TiO₂ exhibited optimal catalytic performance for ethanol oxidation and CO₂ yield by the suppression of SMSI.

Keywords: mesoporous Al-doped TiO₂; Pd/TiO₂; ethanol oxidation; oxide Pd

1. Introduction

Removal of volatile organic compounds (VOCs) has been extensively studied for their formidable harm to human health and to atmospheric pollutions [1-5]. The application of alternative fuel such as ethanol-gasoline dramatically couples reduction of HC and CO emissions with increment of emitted ethanol and other intermediate products [6]. It is of scientific and environmental considerations to investigate ethanol's elimination in detail.

One of the most effective and environmentally friendly purification technology to ethanol-fueled vehicles exhaust is catalytic combustion, through which the unburned ethanol, intermediate acetaldehyde and ester can be oxidized into CO₂ and H₂O [7]. Many research groups have extensively studied complete oxidation of ethanol over the past few decades [8-14]. Among them, large amount attention was devoted to titania (TiO₂), which was widely used as carriers [5]. But traditional TiO₂ supported catalysts can no longer satisfy the need of catalytic performance for their weak thermostability and low specific surface area. Attempts have been made to improve performance of titania by the exploration of mesoporous TiO₂ materials with packed porous [15]. While in preparing mesoporous titania, the structures and properties of the final products could be influenced by two critical issues, one was the retardation of cooperative assembly with templates for the high reactivity of hydrolysis and condensation of titanium precursors, which has been relieved by a method called evaporation induced self-assembly (EISA) [16]. The other lied in the contradiction between framework reservation and single crystal with high crystallinity

during calcination at high temperature to removal surfactants and to promote TiO₂ crystallization [17, 18]. It has been accepted that the addition of metal to TiO₂ could obviously effect phase transformation, consolidate skeletal architecture and improve catalytic performance. Tarek Barakat et al. have investigated T₅₀ of total oxidation of toluene with group V metal oxides doped hierarchically structured macro-mesoporous TiO₂, and the results revealed that doping with Nb₂O₅ and V₂O₅ can enhance the catalytic performance of TiO₂ support [19]. The introduction of aluminium to anatase TiO₂ materials has been demonstrated by many research groups [20-22]. While to the best of our knowledge, literature on the Al doped TiO₂ mesoporous material prepared by structure directing agents is quite rarer than those of pure mesoporous materials such as SiO₂, TiO₂, Al₂O₃ [23-27].

Palladium based catalysts have been confirmed to be highly efficient for catalytic combustion of ethanol [14]. It has been a general consensus that ethanol oxidation over palladium based catalysts is structure sensitive reaction, and the dispersion as well as particle size of palladium are of the predominant factors for catalytic performance [5, 28]. To improve catalytic properties, it is important to obtain smaller size palladium particle. For the existence of the strong metal-support of Pd/TiO₂, researchers have found anomalous chemisorption behavior under reduction atmosphere [29]. In the procedure of oxidation of ethanol, CO and H₂ might be produced and CO has been considered harmful to Pd/TiO₂ catalyst, so it is crucial to reduce the effect of redox species to catalysts. Additionally, the chemisorbed oxygen in the interface could play key role to reaction, it is necessary to boost the diffusion of gaseous phase oxygen from air to the interface of Pd-mesoporous TiO₂ [30, 31]. Nevertheless, even the Pd-based catalysts have been widely used for the catalytic oxidation of most VOCs, there remains a relatively blank field about influence of Al on chemical state and distribution of palladium, on the interaction between Pd and TiO₂ as well as the catalytic performance of ethanol oxidation.

The aim of this work is to prepare Al-doped TiO₂ mesoporous materials by a classical EISA procedure using of triblock copolymer (P123) as structure directing agents and to load Pd by a wet-impregnation method. The catalytic performance was investigated for catalytic oxidation of ethanol, especially the total oxidation to CO₂,

and then the relationship between structure and performance was discussed.

2. Experimental

2.1 Preparation of samples

Procedure to prepare Al doped-TiO₂ mesoporous materials were described in this study, and the synthesis of mesoporous titania was followed a previous EISA method [32]. In a typical synthesis, 4.5 g P123 was dissolved in 26 mL 1-butanol at room temperature. Next, 15 mL tetrabutyl titanate and moderate aluminum iso-propoxide, which was fully grind in a mortar and pestle, were added in turn into the P123 solution slowly and being stirred for 2 h. The solution in another container consisting of well mixed 2.8 mL 37 wt. % hydrochloric acid, 4 mL distilled water and 26 mL 1-butanol was added drop by drop to the above mixture under stirring for 3 h. Then the sol was dried at 50 °C for 48 h and 100 °C for 24 h at a dish, the final gel was heated in air in a muffle oven to 350 °C and 500 °C respectively at a ramp rate of 1 °C/min, the range of Al element loading of (0, 2.5, 5, 7.5 and 10 wt. % Al) and denoted as: T-350, 2.5AT-350, 5AT-350, 7.5AT-350, 10AT-350, while the sample calcined at 500 °C denoted as above but change 350 to 500 just as T-500 and so on.

Palladium was loaded on the carriers calcined at 500 °C by a wet-impregnation method, and the entire samples contained Pd content of 1wt. %, theoretically. The samples prepared in different conditions were denoted as: Pd/ x AT-500 (x=0 with no A, 2.5, 5, 7.5 and 10).

2.2 Activity test

The catalytic performance of the samples was evaluated on a fixed-bed reactor connected with an online gas chromatograph. The compositions of ethanol and products were analyzed on a GC-950 apparatus with two FID detectors, one of which incorporated a methanator. 0.30 g catalyst was being tested (40-60 mesh) with the feed gas consisted of 0.5 vol. % C₂H₅OH, 5 vol. % air and a balance of N₂. The flow

rate was 100 mL/min of total gas and the gas hourly space velocity (GHSV) was 24000 h⁻¹. Ethanol conversion (X_i) and the yields (Y_j) of by-products and carbon dioxide from ethanol combustion were calculated according to the formulas followed:

$$X_i = \frac{C_{i,in} - C_{i,out}}{C_{i,in}} \times 100\% \quad Y_j = \frac{C_{j,out}}{C_{i,in}} \times \frac{1}{n_{ratio}} \times 100\%$$

Where C_i and C_j are the concentrations of ethanol and products from ethanol combustion, respectively, n_{ratio} is the products and reactants carbon atom ratios. And

$$C_i = A_i \times f_i \quad C_j = A_j \times f_j$$

Where A and f are the peak areas and the relative correction factors of reactants (i) or products (j), respectively.

2.3 Characterizations

Low-angle and wide-angle X-ray diffraction (XRD) patterns of all samples were collected in θ - 2θ mode on Rigaku D/MAX-2550 apparatus (Cu $K_{\alpha 1}$ radiation, $\lambda=1.5406 \text{ \AA}$). Intensities of the diffraction peaks were recorded for 2θ range 0.5-80° with a step size of 0.01° and the scanning speed was 8°/min.

Measurement of pore structure from the N₂ adsorption-desorption isotherms were measured on a NOVA 2000e surface area and pore size were analyzer at 77K (liquid nitrogen temperature). Prior to measurement, all samples were degassed at 250 °C for 240 minutes under vacuum. The specific surface areas of the samples were calculated by the Brunauer-Emmett-Teller (BET) method. The mesopore size distribution and total pore volumes were determined using the Barrett-Joyner-Halenda (BJH) method.

Fourier transformed infrared spectroscopy (FT-IR) analysis was carried out using NICOLET360 type spectrometer. The spectra of solids were obtained using KBr pellets. Before measurement, the catalyst and potassium bromide were mixed together in accordance with the quality ratio 1:100. The vibrational transition frequencies are reported in wave numbers (cm⁻¹).

Transmission electron microscopy (TEM) and high resolution transmission electron micrographs (HRTEM) were carried out on JEOL-2100F electron

microscope, operating at 200 kV.

Hydrogen temperature-programmed reduction (H₂-TPR) was performed on an AutoChem II 2920 chemisorption analyzer (Micromeritics, Norcross, GA, USA) equipped with a TCD detector. A 100 mg catalyst sample was pretreated at 300 °C for 0.5 h in N₂ atmosphere to remove the adsorbed matters. After cooling to room temperature, the sample was exposed to a flow of 10 Vol. % H₂/90 Vol. % Ar (50 mL/min), and the temperature was increased linearly at 10 °C/min.

X-ray photoelectron spectroscopy (XPS) analysis was conducted on a Kratos Axis Ultra DLD multifunctional surface analysis photoelectron spectrometer with X-ray source at 450 W and Al-K α radiation (1486.6 eV). The element binding energies were referenced to the C 1s line at 284.6 eV and measurements were restricted an estimated error of ± 0.1 eV.

Pulse H₂ chemisorption on a Micromeritics AutoChem II 2720 with TCD to monitor H₂ consumption was used to determined surface Pd atoms exposed on the surface. Before measurement, 0.1g sample was pretreated by helium flow for 1 h at 200°C to remove gaseous species adsorbed, and then cooling down to 60°C. The calculation of turnover frequencies (TOF) based on ethanol conversion (TOF_i), product generation (TOF_j) and the amount of Pd atoms. A H₂/Pd average stoichiometry of 1 has been assumed [33]. The turnover frequencies of Pd catalysts were calculated as follows

$$TOF_i = \frac{C_i X_i V_{i,in}}{n_{Pd}} [s^{-1}] \quad TOF_j = \frac{Y_j C_i V_{i,in}}{n_{ratio} n_{Pd}} [s^{-1}]$$

Where C_i is the concentration of ethanol in gas mixture; X_i is the conversion of ethanol; V_{gas} is the total gas flow rate; n_{Pd} is the mole number of Pd atom calculated by pulse H₂ chemisorption. And in our work, the initial concentration of ethanol in gas mixture, total gas flow rate, reaction time and mass of catalyst are the same, respectively.

3. Results and discussion

3.1 Evaluation of the catalytic activity

Fig. 1 shows the temperature dependence of total oxidation of ethanol for the Al doped 1 wt. % Pd/ xAT-500 and Pd/T-500 catalysts from ambient temperature to 450 °C. On different amount of Al doping TiO₂ supported Pd catalysts, it can be found the activities of ethanol oxidation over TiO₂ supported Pd catalysts were greatly improved by the introduction of aluminium. It is obviously to see that at reaction temperature of 200 °C, the conversion of ethanol over Pd/7.5AT-500 has reached 69.5 %, which is apparent higher than that over Pd/T-500. At the same temperature point, CO₂ yield over Pd/7.5AT-500 was 68.0 %, which was significantly higher compared with that over others. To further gain insight into the relation between active Pd atom and catalytic efficiency, turnover frequencies of Pd/7.5AT-500 and Pd/T-500 were calculated on the basis of ethanol conversion and product yield and the amount of active site measured by H₂-pulse chemisorption are shown in Table.1. It can be seen the TOFs of ethanol conversion (TOF_i) and CO₂ generation (TOF_j) over Pd/7.5AT-500 is significantly higher than that over Pd/T-500. Compared with Pd/T-500, the Pd/7.5AT-500 obtained much higher TOF_i and TOF_j at the same temperature, which means the higher ethanol oxidation and CO₂ production from ethanol oxidation per unit time on per active sites. Especially, at reaction temperature of 200°C, the ratio of TOF_i (3.17 s⁻¹) and TOF_j (1.62 s⁻¹) of Pd/7.5AT-500 is 1.96 which is very close to carbon atom ratio of ethanol and CO₂ which means ethanol molecular involved in reaction largely converted to CO₂, while that over Pd/T-500 is 1.62, thus the enhanced catalytic efficiency was obtained at the Pd/7.5AT-500. These results suggest that the Pd/TiO₂ with aluminium achieved much higher reactivity than TiO₂ without dopants prepared by EISA supported Pd catalysts. What worth noting is that no CO was observed on the Pd/7.5AT-500 catalyst through the whole reaction of ethanol (shown in Fig.S1). While as addressed before, acetaldehyde and CO were the main by-products for the catalyst with low content of noble metal loading [34]. The

doping of Al could influence the reaction path of oxidation of ethanol. The yields of other by-products showed no significant differences.

Fig. 1. Ethanol conversion and curves for Yields to CO₂ Pd/T-500 and Pd/xAT-500 prepared by aluminium doped TiO₂ mesoporous material supported 1wt. % Pd

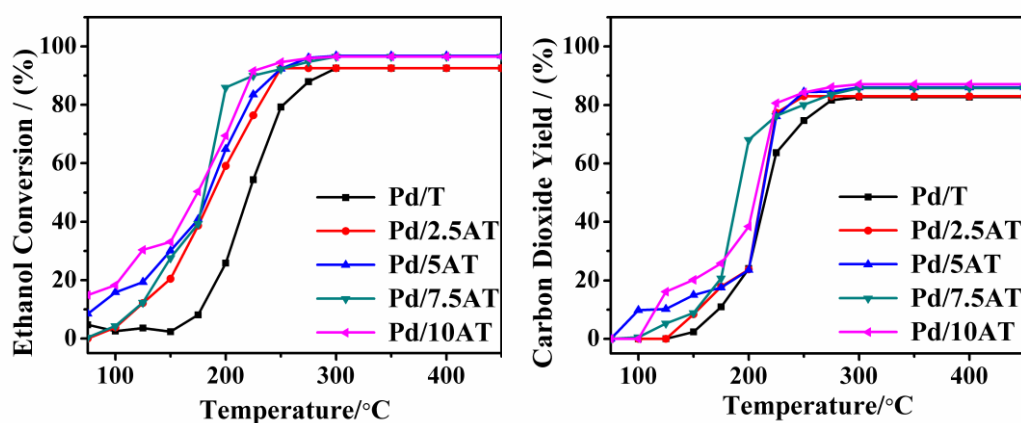


Table 1 TOFs of Pd/T-500 and Pd/7.5AT-500 for ethanol oxidation.

Tem. °C	TOF ^a of Pd/T-500 (10 ⁻¹ , S ⁻¹)				TOF ^a of Pd/7.5AT-500 (10 ⁻¹ , S ⁻¹)			
	Con.%	TOF _i ^b	Yield %	TOF _j ^c	Con.%	TOF _i ^b	Yield%	TOF _j ^c
75	4.7	0.30	0	0	14.8	3.45	0	0
100	3.5	0.23	0	0	18.2	4.25	0.6	0.26
125	3.5	0.23	0	0	30.3	7.05	5.3	2.46
150	2.3	0.15	1.4	0.17	33.0	7.68	10.8	5.02
175	9.1	0.58	9.0	1.14	50.3	11.70	21.7	10.11
200	25.8	1.66	21.1	2.69	69.5	16.16	68.5	31.65
225	64.4	4.13	62.8	8.16	91.6	21.31	78.3	36.42
250	79.2	5.08	74.7	9.57	94.6	22.01	81.1	37.69
275	87.9	5.64	81.7	10.47	96.0	22.32	83.6	38.89
300	92.6	5.93	82.7	10.60	96.6	22.44	85.8	39.90

350	92.6	5.935	82.7	10.60	96.6	22.44	85.8	39.90
400	92.6	5.93	82.7	10.60	96.6	2.244	85.8	39.90
450	92.6	5.93	82.7	10.60	96.6	22.44	85.8	39.90

^aTOF= turnover frequency (ethanol oxidation activity per surface Pd atoms sites as measured by H₂ pulse chemisorption.

TOF_i^b = turnover frequency of ethanol conversion

TOF_j^c = turnover frequency of CO₂ production

3.2 XRD analysis

To identify structure of ordered mesoporous materials, low-angle XRD were carried out for all the materials contained different content of aluminium. As shown in Fig. 2a. All samples exhibits a diffraction peaks at 2θ value about 1.2° and an additional broad peak at range 2.0 - 2.5° indicate the mesoporous structure with short range order [22, 35]. Comparatively, the peak intensity between Al-doped samples and undoped one have a certain extent improvement, suggesting the introduction of aluminium improves the order of the mesoporous structure. While the peak at 1.2° corresponding to the d-spacing of 7.36 nm. And the wide-angle X-ray diffraction patterns of different content Al-doped TiO₂ mesoporous nanocomposites calcined at 350 °C are shown in Fig. S2. In comparison with pure TiO₂, the patterns of Al doped TiO₂ samples indicate a low level crystallinity of anatase. While an increase in the broadening peaks of the (101) anatase peak with increasing dopant of Al can be observed for all concentrations. Different carries with improved crystallinity when calcination temperature was risen to 500 °C can be seen in Fig. 2b. And evidence for template removal of samples has been confirmed by FT-IR (Fig. S3). According to PDF#73-1764, the major crystal phase of supports is anatase while the weak diffraction peak at around 27.4° on pure TiO₂ is assigned to rutile, indicating that phase transformation occurred in preparing TiO₂ mesoporous material with EISA procedure under certain condition. However, no signal of rutile phase can be seen for supports contain aluminium. Apparently, the introduction of aluminium inhibits the

formation of rutile from anatase phase during heat treatment at 500 °C. What counts on most is that anatase was confirmed a favourable factor to promote catalytic reaction.

On the other hand, the diffraction peak observed at palladium based catalysts at 2θ position of around 33.6° can be indexed to PdO (JCPDS75-0584) [36, 37]. While no peak related to metallic Pd can be observed, and this may due to the low content. In the meantime, no characteristic diffraction peaks for individual aluminium species are observed in the samples. By comparing the full width at half-maximum (FWHM) of the strongest diffraction peak at around 25.4° , it is found that the (101) plane of Al-doped sample exhibits 2-fold higher FWHM value than pure TiO₂. It has been certified that XRD peaks become less sharper when the grain size decreases or the crystallinity reduced [25, 38]. According to the (101) plane of anatase phase, the average crystallite sizes of all samples were estimated according to the Scherrer equation (Table 2). For all the supports calcined at 500 °C, the crystallite sizes of anatase phase of TiO₂ can be roughly summarized to be about 16 to 9 nm. The mean size of 7.5AT-500 achieves the relatively small one of 9.06 nm, meaning the introduction of moderate amount of aluminium can embarrass the grain growth of anatase.

Fig. 2 Low-angle XRD patterns (a) of TiO₂ and Al-doped TiO₂ mesoporous materials calcined at 500 °C and wide-angle XRD patterns (b) of mesoporous materials and catalysts Pd/T-500 and Pd/7.5AT-500 (a) and wide-angle (b)

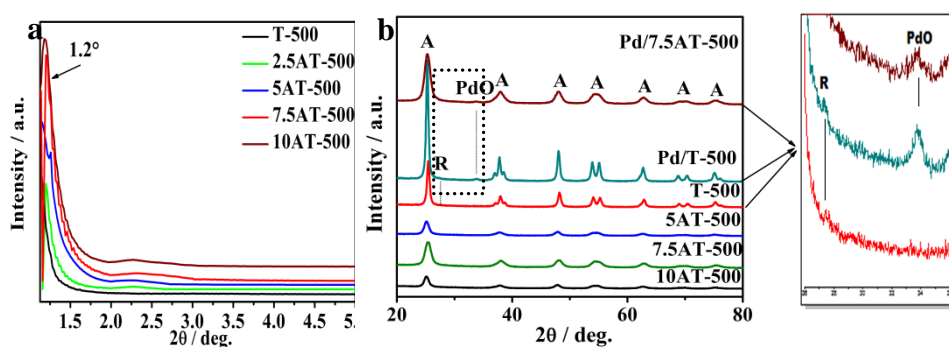


Table 2 Phase content, FWHM and crystallite size of supports and catalysts

sample	anatase Content (wt. %)	anatase FWHM (°)	anatase Crystallite Size (nm)
10AT-500	100	0.72	11.11
7.5AT-500	100	0.89	9.06
5AT-500	100	0.78	10.38
T-500	98.37	0.45	16.14
Pd/7.5AT-500	-	0.87	9.23
Pd/T-500	-	0.44	18.17

3.3 Measurement of pore structure

N₂ adsorption-desorption isotherm measurements were used to analyze the mesoporous structure of the samples calcined at 500 °C, and the curves are shown in Fig. 3. The BET specific surface areas, pore volumes and pore sizes are listed in Table 2.

The N₂ adsorption-desorption isotherms on samples present similar appearance of a flat “S”-shape of type IVa curves with a clear absorption hysteresis loop located at $0.40 < P/P^0 < 1.0$ of H2-type hysteresis loops according to IUPAC classification, indicating the presence of “ink-bottle” mesopores [39]. The capillary condensation stage on curves of samples contain 7.5 wt. % aluminum have distinct sharp adsorption trend compared to pure TiO₂, revealing the existence of narrow pore size distribution and relatively uniform channel in agreement with BJH pore-size distribution patterns of Fig. 3 (insert). It could be found from data of Table 3 that the BET specific surface area changes extremely when moderate aluminium were added to support material and catalysts, respectively. The low BET surface area and broad pore size distribution of pure TiO₂ calcined at 500 °C remain practically constant with literary [40]. In contrast, pore size of 7.5AT-500 is 4.28 nm, smaller than pure TiO₂ (4.87 nm), in respect that rutile between intra anatase grains would expand primary interspace for rutile possess larger volume, the introduction of aluminium inhibits fast crystallization and phase transformation of anatase to rutile, as a result the relatively smaller pore

were preserved [41].

Consequently, the mesochannel and enhanced stabilized anatase (according to XRD results) can be retained to supply the efficient transport pathway for reactants and products, which is propitious to the high catalytic activity. After loading of palladium, interestingly, samples with and without aluminium present the opposite trends, it is noticeable that an instinct decrease of BET surface area (from 159.39 m^2/g^{-1} to 98.67 m^2/g^{-1}) pore size (from 4.28 nm to 3.39 nm) and pore volume (from 0.14 $\text{cm}^3/\text{g}^{-1}$ to 0.13 $\text{cm}^3/\text{g}^{-1}$) can be observed, indicating the successful incorporation of palladium species into the mesoporous architecture of the supports [41]. Reference accounted that high surface area and pore volume consisted with open aperture and short channel length can benefit absorption and mass transfer of reactant molecules, reduce the diffusion distance of product molecules in the pores and the probability of the occurrence of secondary reactions, and improve anti-coking ability of the catalyst as well as the stability of charcoal [42, 43].

Fig. 3 N_2 adsorption-desorption isotherms and pore size distributions (insert) of pristine mesoporous TiO_2 (T-500), 7.5 wt. % aluminium doped TiO_2 mesoporous material (7.5AT-500). 1 wt. % Pd/ TiO_2 (Pd/T-500) and 1 wt. % Pd/7.5AT (Pd/7.5AT-500)

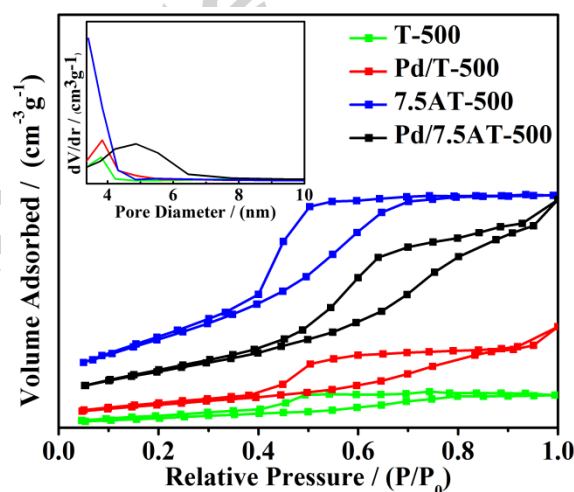


Table 3 Textural properties of supports and catalysts

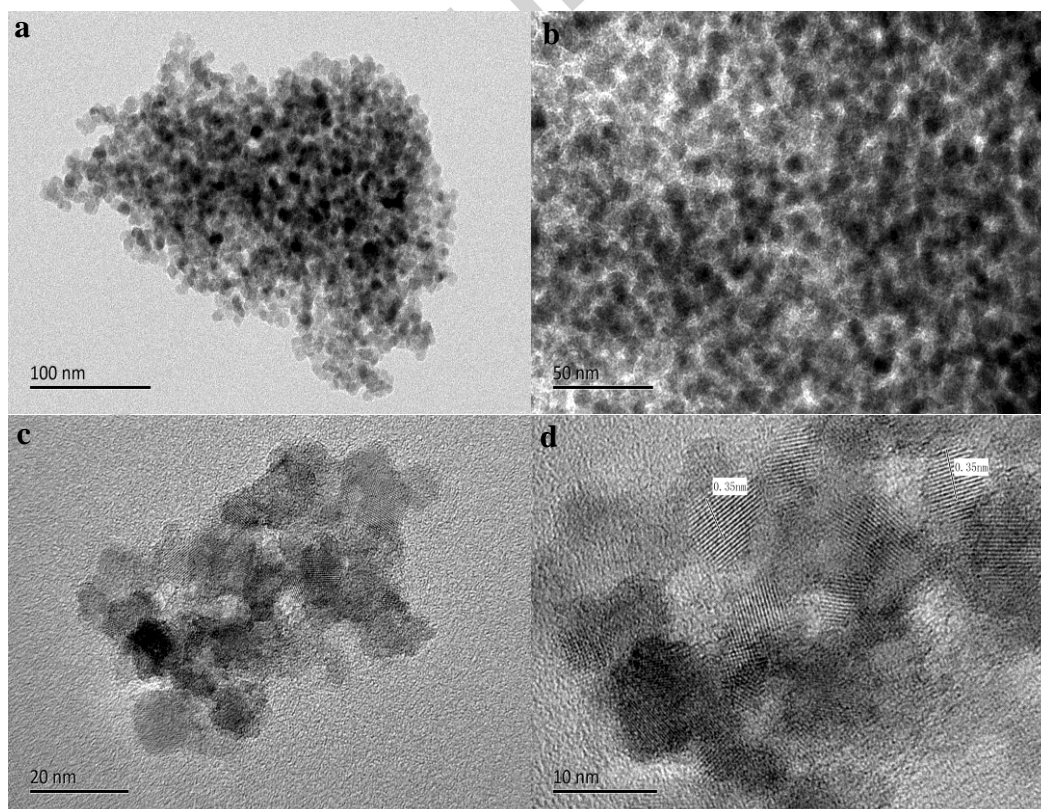
sample	S_{BET} (m^2/g^{-1})	V ($\text{cm}^3/\text{g}^{-1}$)	D_{pore} (nm)
--------	---	-------------------------------------	------------------------

T-500	18	0.02	4.87
Pd/T-500	40	0.07	6.50
7.5AT-500	159	0.14	4.28
Pd/7.5AT-500	98	0.13	3.39

3.4 Transmission electron microscopy (TEM)

Typical TEM and HRTEM images of 1 wt. % palladium loaded 7.5 wt. % aluminium-doped TiO_2 are shown in Fig. 4. It can be seen that the mesoporous structure has been successfully retained [22]. The lattice fringe of the selected particles is 0.35 nm, which belongs to the spacing of anatase. The TiO_2 particles have a size about 9 nm, which is consistent with the XRD data. Some metal agglomeration could be observed while it is difficult to distinguish Pd/PdO clusters/particles on the Al-doped TiO_2 mesoporous material supported palladium catalyst [44].

Fig. 4 TEM and HRTEM imagers of Pd/7.5AT -500 prepared by 7.5 wt. % aluminium doped TiO_2 mesoporous material supported 1 wt. % Pd



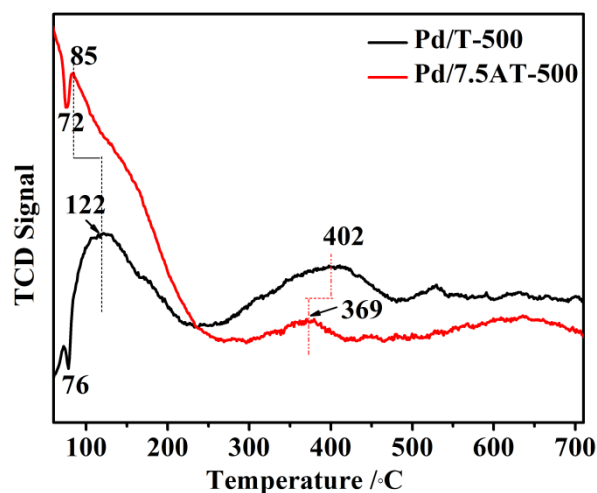
3.5 H₂-TPR analysis

H₂-TPR measurements were carried out to identify Pd species and interaction between Pd and supports. The TPR profiles of Pd catalysts supported on TiO₂ and Al doped-TiO₂ are shown in Fig. 5

A negative H₂ consumption peak at around 75 °C can be observed because formation of β-PdH in treatment with H₂/Ar mixture at room temperature and it could be decomposed to H₂ below 100 °C [45, 46]. The slight shift to lower temperature of Pd/7.5AT-500 compared with Pd/T-500 could be attributed to the weak extent of the strong metal-support interaction (SMSI) [47]. The reduction peak at around 85 °C for Pd/7.5AT-500 is most likely due to reduction of Pd oxide to Pd metal, which is significantly lower than that of Pd/T-500 meaning the Pd oxides is more reducibility on Pd/7.5AT-500 than that of Pd/T-500. Actually, it has been convinced that defective structures of TiO₂ caused by dopants with oxidation state lower than tetravalence could produce vacancies considered to arouse higher lattice oxygen mobility thus enhance reduction of Pd species [48]. So the significant lower reduction temperature and asymmetric peak at 85 °C for Pd/7.5AT-500 might be related to the increased number of titania defects. Further characteristic method should be applied to identify existence of defected TiO₂. And the third peak corresponded to the reduction of surface TiO₂ particles [49, 50]. From the peak intensity and temperature range, the amount of hydrogen consumption for TiO₂ reduction on Pd/T-500 is significantly higher than that on Pd/7.5AT-500. The different degree of SMSI over Pd catalysts was observed by the TiO₂ reduction pattern. It has been demonstrated that Pd particle on the surface could be decorated by TiO₂ overlayer and promotes TiO₂ reduction more vigorously in precious study which is consistent with observation in our Pd/T-500 [51]. The SMSI state Pd atom of Pd/T-500 can adopt electron from TiO₂ and form electron-rich metal which might be hard to be oxidized in the catalytic cycle and left a large amount of TiO_x. The reducibility of Palladium species could be weakened. In general, alcohol oxidation

has close relation with reducibility of active component. The lower reduction temperature of small palladium oxides particles have easier access to higher catalytic performance [52]. And based on the H₂-TPR results, the introduction of aluminium could suppress the SMSI and hence the reducibility of palladium species. The more readily reducible palladium species exhibits facile approach reduction and oxidation cycle in the catalytic process. The results properly supported the conclusion that the introduction of aluminium can weaken the metal-support interaction between Pd and TiO₂.

Fig. 5 H₂-TPR profile of Pd/T-500 and Pd/7.5AT-500 prepared by 7.5 wt. % aluminium doped TiO₂ mesoporous material supported 1 wt. % Pd



3.6 XPS evaluate

To deep investigate the influence of doping element on catalyst, we analyzed changes in oxidation state by X-ray photoemission spectroscopy (XPS) to provide information on surface segregation of Pd based 7.5 wt. % Al species doped TiO₂ and Pd/T-500. Characteristic XPS of survey spectra and core level single spectra of the bonding partners are presented in Fig. 6 (a-f).

Fig. 6a shows the wide survey scan of the samples, compared to curve of Pd/T-500, Al-doped sample presents obvious peak of Al species, and binding energies of 74.6 and 118.6 eV in the spectra correspond to the photoelectron peak of Al 2p and Al 2s, respectively, which can be ascribed to the formation of Al³⁺ [53]. Furthermore,

high resolution XPS of Al 2p (Fig. 6b) presents that the main peak at around 74 eV is in accordance to aluminium ions situating in the TiO₂ lattice as Ti-O-Al structure [54-56].

Fig. 6c shows the Ti 2p curves of Pd based Al-doped and undoped TiO₂ mesoporous materials and details for the peak fitting parameters are presented in Fig. S4a. For spin-orbit coupling effect, the Ti 2p core level could split into 2p_{3/2} and 2p_{1/2} with binding energies of 458.4 eV and 463.9 eV, respectively. Due to the pronounced asymmetry of peaks, curves were decomposed into several contributions due to Shirley background and Caussian-Lorentzian fitted method related to oxidation states of Ti possess. For each doublet, the ratio of the area of the two peaks A(Ti 2p_{1/2})/A(Ti 2p_{3/2}) was equal to 1/2 and the binding energy separation between Ti 2p_{1/2} and Ti 2p_{3/2} in the same valence conditions was kept in the region of 5.6-5.7 eV, which are in agreement with previous literature [56]. The Ti 2p curve shows the existence of Ti³⁺ and Ti⁴⁺ in catalyst of Pd/T-500. The peaks at 458.6 eV (2p_{3/2}) and 464.3 eV (2p_{1/2}) signify the appearance of Ti tetravalent ions, besides, the two at lower binding energy of 456.3 eV (2p_{3/2}) and 462 eV (2p_{1/2}) are attributed to the existence of Ti³⁺ [22, 57, 58]. The peak at 457.4 eV is the satellite peak of titanium species. While it is worth noting that only peaks related to Ti⁴⁺ species can be observed in Pd/7.5AT-500. The additional peak at 459.3 eV is a characteristic of Ti species in oxidation state related to Al (probably Al₂TiO₅) [59]. We speculate that the presence of Ti³⁺ might be due to the reducibility of TiO₂, especially when connected with Pd. SMSI effect for TiO₂, titanium oxides would migrate on the surface of metal, which induces charge transfer on metal-support [60]. The binding energy of Ti 2p_{3/2} peak (Ti⁴⁺) shifts slightly to a lower position (by 0.3 eV) compared Pd/7.5AT-500 with Pd/T-500, and this negative shift suggests the existence of more serious TiO₂ defect, regarding that the chemisorption of oxygen atom can be enhanced on the vacancy of defected TiO₂ [31].

According to high resolution Pd 3d XPS spectrum in Fig. 6d and details for the peak fitting parameters in Fig. S4b, oxidation states of Pd and relative amount can be obtained. A Pd 3d_{5/2} peak at 336.4 eV for both doped and undoped palladium catalysts corresponds to Pd²⁺. The binding energy of 334.4 eV in Pd/T-500 can be assigned to

metallic Pd⁰, and Pd⁰ is not detected on Pd/7.5AT-500 but a peak at 337.6 eV belonging to Pd⁴⁺ is presented [61-63]. In the case of Pd/T-500, the binding energy of Pd⁰ is slightly shifted to lower binding energy (around 0.5 eV) compared to data reported before, revealing that electrons are donated from TiO₂ to Pd, which can be another indicative of SMSI as reported before [64, 65]. This SMSI effect is higher in Pd/T-500 than in Pd/7.5AT-500, meaning the introduction of aluminium can suppress the interaction on Pd and TiO₂.

The O 1s spectrum of Fig. 6e and fitting parameters listed in Fig. 6f are used to show the types of surface oxygen species in the catalysts. According to the photoelectron peak positions and literatures reported before, the high binding energy peak is assigned to surface adsorbed oxygen. It can be seen, O 1s spectrums reveal apparent shoulder peak at 531.2 eV (named O_{II}) on both one which should be ascribed to the adsorbed oxygen on the surface of palladium catalysts. The doped catalyst possess higher capacity of adsorbed oxygen than the undoped one, this can be attributed to the serious TiO₂ defect (as evidenced by XPS of Ti 2p). Chemisorption oxygen were considered presented high mobility and deep involved in the VOCs removal [66]. In addition, the binding energy peak at about 529 eV is related to oxygen atom linked to Ti⁴⁺ and the binding energy of 527.6 eV is ascribed to one linked to Ti³⁺ which can only be detected in undoped catalyst [62, 67]. The unknown feature at around 528.5 eV marked by sat.

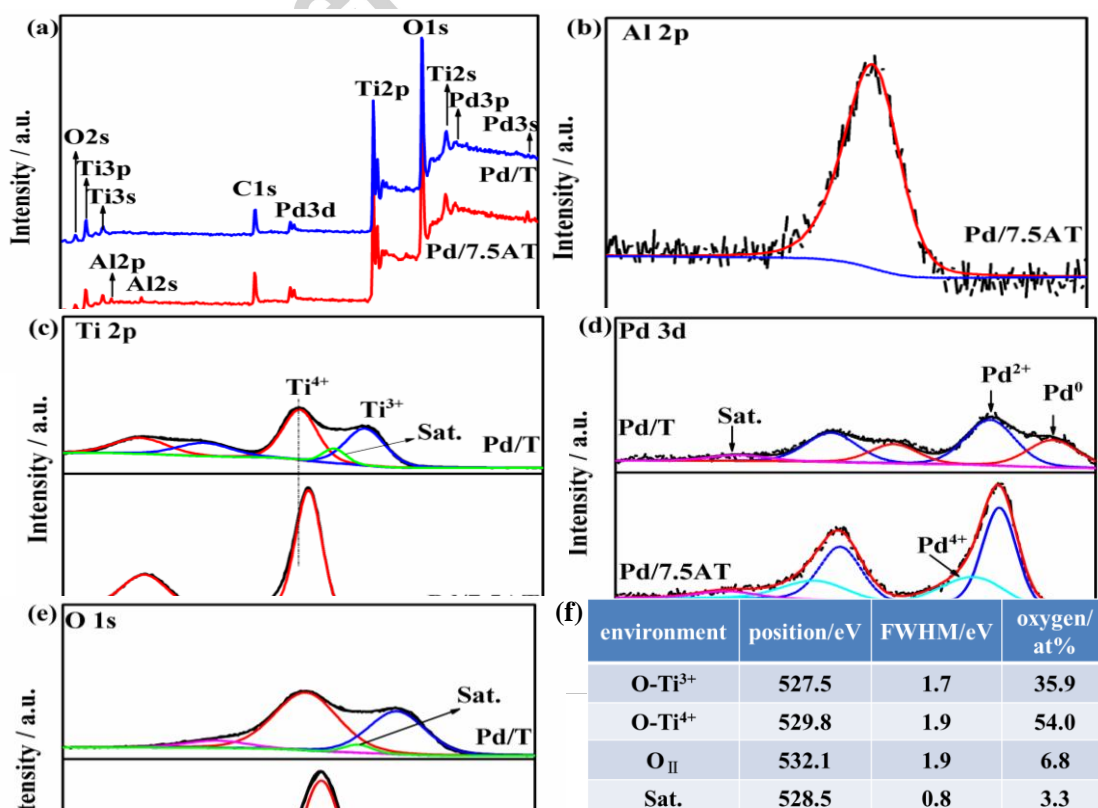


Fig. 6 XPS spectra of Pd/T-500 and Pd/7.5AT-500 prepared by 7.5 wt. % aluminium doped TiO₂ mesoporous material supported 1 wt. % Pd :(a) survey spectra; (b) Al2p spectrum (c) Ti2p spectrum; (d) Pd3d spectrum;(e) O1s spectrum; (f) peak fitting parameter for O1s spectrum

3.8 Discussion on influence of Al doping

According to all the observations and the literature, there is a bold speculation accounted for the correlation between Al dopant and ethanol oxidation.

As shown in Table 1. The catalytic efficiency of Pd/T-500 is significantly lower than Pd/7.5AT-500 correlated to ethanol conversion and CO₂ production based on TOFs and shown in Table 1 at low temperature. The enhanced catalytic activities should be attributed to aluminium dopants. It is essential to figure out why and how aluminium influences the catalytic activity. It has been proven previously that the combination or at least one of stabilized anatase of TiO₂, activated cationic metal /metal component and abundant adsorbed oxygen could lead to high activity [30, 31]. The results of XRD (Fig. 2a) and XPS pattern indicate that both (i) the stabilized anatase with relative high surface area and (ii) cationic Pd and abundant adsorbed oxygen are presented in Pd/7.5AT-500. While how this positive influence of the introduction of aluminium on catalyst properties and catalytic activity are discussed below. There are two possible reasons for the optimal performance of Pd/7.5AT-500. One is the surface different atom ratio, for there is an optimum metal/titania ratio below which would induce the charge recombination in TiO₂, while on the contrary,

the high metal contents would increase recombination at metal particles which endure adverse effect [68]. In addition to metal/titania ratio, oxygen/titania ratio can affect catalytic performance, for that below stoichiometric value of 2.0 (TiO_2) would increase the formation of oxygen vacancies and decrease electron hole recombination rate [64]. To determine the surface atomic ratio for the catalytic performance, we calculated the surface Pd/Ti and O/Ti of the Al-doped sample and that of pure TiO_2 (Table 4). For the Al-doped catalyst, the Pd/Ti ratio was found to be 0.06, just a little higher than that of Pd/T-500, while the O/Ti ratio was 3.29, and that of Pd/T-500 was 3.00. These variations are not convictive enough to explain such an increased catalytic performance on the oxidation of ethanol.

Table 4 Surface atom ratio from XPS

Sample	Pd/Ti	atomic %	O/Ti	atomic %
Pd/T-500	0.04		3.00	
Pd/7.5AT-500	0.06		3.29	

The other reason lies in the strong metal-support interaction between palladium and TiO_2 . SMSI between Pd and TiO_2 after exposure to air at relatively high temperature should exist for the reducibility of TiO_2 , which has been observed by Ouyang [69]. To identify the effect of introduction of aluminium on SMSI, it is necessary to distinguish whether the doped Al cation situated at Ti substitution sites or interstitial sites [70]. If Al^{3+} is incorporated into interstitial void of anatase lattice, the lattice parameters will increase and the diffraction peaks will shift to lower angle region in the XRD patterns [53, 54]. In our paper, the peak of anatase (101) appears at 25.42° for the 7.5 wt. % Al doped TiO_2 , which is a little higher than that of 25.28° for the undoped one, indicating trivalence Al has substituted Ti^{4+} in the anatase lattice [71]. The shift of binding energy related to Ti $2p_{3/2}$ of Ti^{4+} to lower position (by 0.3 eV) is consistent with the wide-angle XRD results. Determined by electron structure of doped ions, new energy level might be formed in pristine material. Charge transfer from Al^{3+} to Ti^{4+} would inhibit phase transformation, and this can suppress the reduction atmosphere and electron transfer between metal and support, which could

result in lower SMSI. It can be seen that the amount of the Pd²⁺ state is approximately 60% in both doped and undoped catalysts. And the percent of Pd⁰ in Pd/T-500 and Pd⁴⁺ in Pd/7.5AT-500 possess almost unanimously, respectively. Therefore as detected by XPS, the introduction of Al leads to the transformation of low valence Pd to higher valence Pd species. Given that the species of active sites correlates with catalytic performance of ethanol oxidation, high valence cationic Pd is much more active than metallic one.

Based on the presence of Ti (IV) and cationic Pd with higher valence, it is reasonable to propose that the introduction of Al produce an obvious negative effect on SMSI. The catalytic system of Pd/T-500, possessing a SMSI effect higher than Pd/7.5AT-500, is less effective in terms of ethanol oxidation and CO₂ yield, in contrast to the improvement effect of SMSI of Pd/T-500 reported recently for HCHO oxidation [66]. This adverse result suggests that the effect of SMSI on VOCs oxidation may be connected with the VOC species. Based on surface reaction mechanism, on the surface of catalyst, ethanol would be dehydrogenized into ethoxyl, and then ethoxyl would be further oxidized into CO₂ and H₂O at the presence of oxygen [14]. Catalytic system with lower SMSI is more effective in terms of dehydrogenation from organics [64]. The introduction of aluminium produces a boost of ethanol oxidation might be ascribed to the allocation of Pd oxides and the higher reducibility Pd oxides exhibit facile approach reduction and oxidation cycle in the catalytic process. And detailed research about effects of metal oxide-support interaction on approach of ethanol oxidation should be carried out.

4. Conclusions

In our contribution, we have reported a wet impregnation assisted EISA procedure to prepare palladium catalysts supported on Al doped anatase TiO₂ mesoporous materials. Aluminium has been incorporated into anatase TiO₂ framework by substituting Ti⁴⁺ ions and this introduction brought about anatase monocrystalline, narrow mesoporous size dispersion and high specific surface area of Pd catalyst. The

obvious decrease of initiation temperature and optimal catalytic performance on reaction temperature below 200 °C were observed for ethanol conversion and CO₂ production on the doped Pd/AT-500 relative to undoped one, which could be attributed to the new properties of Al-doped TiO₂. We proposed that the introduction of Al suppresses the charge transfer from TiO₂ to Pd (SMSI) and facilitates Pd oxides which has higher reducibility act as catalytically active sites, and the abundant chemisorption oxygen generated on the defected mesoporous TiO₂ is beneficial for surface ethoxyl to form CO₂ and H₂O.

Conflict of Interest:

The authors declare that they have no conflict of interest.

Acknowledgements:

The authors gratefully acknowledge the Project supported by the State Key Program of National Natural Science of China (Grant No. 21336006) and Shanxi Province Scientific and Technological Project (20140313002-2).

Reference

- [1] A. George, O. Evaggelos, K. Dimitrios, T. Ioannides, *Appl. Catal. B: Environ.* 65 (2006) 62-69.
- [2] A. Aranzabal, M. Romero-Sáez, U. Elizundia, J.R. González-Velasco, J.A. González-Marcos, *J. Catal.* 296 (2012) 165-174.
- [3] R. Wang, J. Li, *Environ. Sci. Technol.* 44 (2010) 4282-4287.
- [4] N.A. Merino, B.P. Barbero, P. Ruiz, L.E. Cadús, *J. Catal.* 240 (2006) 245-257.
- [5] V.P. Santos, S.A.C. Carabineiro, P.B. Tavares, M.F.R. Pereira, J.J.M. Órfão, J.L. Figueiredo, *Appl. Catal. B: Environ.* 99 (2010) 198-205.
- [6] J. Lacey, K. Kameshwaran, Z. Filipi, W. Cannella, P. Fuentes-Afflick, *Fuel* 126 (2014) 122-133.
- [7] B. Bai, J. Li, J. Hao, *Appl. Catal. B: Environ.* 164 (2015) 241-250.
- [8] H. Rajesh, U.S. Ozkan, *Ind. Eng. Chem. Res.* 32 (1993) 1622-1630.
- [9] R.W. McCabe, P.J. Mitchell, *Ind. Eng. Chem. Prod. Res. Dev.* 23 (1984) 196-202.
- [10] R.W. McCabe, P.J. Mitchell, *Ind. Eng. Chem. Prod. Res. Dev.* 22 (1983) 212-217.
- [11] G. Groppi, C. Cristiani, L. Lietti, C. Ramella, M. Valentini, P. Forzatti, *Catal. Today* 50 (1999)

- 399-412.
- [12] D.I. Enache, J.K. Edwards, P. Landon, B. Solsona-Espriu, A.F. Carley, A.A. Herzing, M. Watanabe, C.J. Kiely, D.W. Knight, G.J. Hutchings, *Science* 311 (2006) 362-365.
- [13] P.-O. Larsson, A. Andersson, *J. Catal.* 179 (1998) 72-89.
- [14] Y.-F.Y. Yao, *Ind.Eng.Chem.Process Des.Dev* 23 (1984) 60-67.
- [15] D.M. Antonelli, J.Y. Ying, *Angew. Chem. Int. Ed. Engl.* 34 (1995) 2014-2017.
- [16] P. Yang, D. Zhao, D.I. Margolese, B.F. Chmelka, G.D. Stucky, *Nature* 396 (1998) 152-155.
- [17] W. Li, Z. Wu, J. Wang, A.A. Elzatahry, D. Zhao, *Chem. Mater.* 26 (2014) 287-298.
- [18] L. Mahoney, R. Koodali, *Materials* 7 (2014) 2697-2746.
- [19] T. Barakat, J.C. Rooke, M. Franco, R. Cousin, J.-F. Lamonier, J.-M. Giraudon, B.-L. Su, S. Siffert, *Eur. J. Inorg. Chem.* 2012 (2012) 2812-2818.
- [20] J. Rubio, J. Oteo, M. Villegas, P. Duran, *J. Mater. Sci.* 32 (1997) 643-652.
- [21] Y.J. Choi, Z. Seeley, A. Bandyopadhyay, S. Bose, S.A. Akbar, *Sensor Actuat B: Chem* 124 (2007) 111-117.
- [22] S. Liu, G. Liu, Q. Feng, *J. Porous Mater.* 17 (2010) 197-206.
- [23] U.O.A. Arter, F.Z. Tepehan, *Compos Part B: Eng* 58 (2014) 147-151.
- [24] S. Badoga, R.V. Sharma, A.K. Dalai, J. Adjaye, *Ind. Eng. Chem. Res.* 53 (2014) 18729-18739.
- [25] X. Dai, J. Liang, D. Ma, X. Zhang, H. Zhao, B. Zhao, Z. Guo, F. Kleitz, S. Qiao, *Appl. Catal. B: Environ.* 165 (2015) 752-762.
- [26] G. Zhu, B. Yang, S. Wang, *Int. J. Hydrogen Energy* 36 (2011) 13603-13613.
- [27] M.A. Ahmed, M.F. Abdel-Messih, *J. Alloys Compd.* 509 (2011) 2154-2159.
- [28] E. Wang, J. Xu, T. Zhao, *J Phys Chem C* 114 (2010) 10489-10497.
- [29] G. Sankar, K. Kannan, C. Rao, *Catal. Lett.* 8 (1991) 27-36.
- [30] H. Huang, X. Ye, H. Huang, L. Zhang, D.Y.C. Leung, *Chem. Eng. J.* 230 (2013) 73-79.
- [31] M.D. Rasmussen, L.M. Molina, B. Hammer, *J. Chem. Phys.* 120 (2004) 988-997.
- [32] S. Yuan, Q. Sheng, J. Zhang, F. Chen, M. Anpo, *Mater. Lett.* 58 (2004) 2757-2760.
- [33] J. Peng, S. Wang, *Appl. Catal. B: Environ.* 73 (2007) 282-291.
- [34] L. Matějová, P. Topka, L. Kaluža, S. Pitkääho, S. Ojala, J. Gaálová, R.L. Keiski, *Appl. Catal. B: Environ.* 142-143 (2013) 54-64.
- [35] J. Du, Z. Liu, Z. Li, B. Han, Y. Huang, Y. Gao, *Micropor. Mesopor. Mater.* 83 (2005) 19-24.

- [36] W. Li, Z. Qiang, T. Zhang, X. Bao, X. Zhao, *J. Mol. Catal. A: Chem.* 348 (2011) 70-76.
- [37] B. Wen, J. Jia, W.M. Sachtler, *J Phys Chem B* 106 (2002) 7520-7523.
- [38] N. Yao, H. Ma, Y. Shao, C. Yuan, D. Lv, X. Li, *J. Mater. Chem.* 21 (2011) 17403.
- [39] M. Thommes, K. Kaneko, A.V. Neimark, J.P. Olivier, F. Rodriguez-Reinoso, J. Rouquerol, K.S.W. Sing, *Pure Appl. Chem.* 87 (2015).
- [40] B. Braconnier, C.A. Pérez, S. Lambert, C. Alié, C. Henrist, D. Poelman, J.-P. Pirard, R. Cloots, B. Heinrichs, *Micropor. Mesopor. Mater.* 122 (2009) 247-254.
- [41] H. Min, X. Ran, J. Fan, Y. Sun, J. Yang, W. Teng, W.-x. Zhang, G. Li, D. Zhao, *J. Mater. Chem. A* 3 (2015) 7399-7405.
- [42] Y. Min, H. Si, W. Jian, D. Tao, W. Yong-Ping, *Acta-Phys.-Chim.Sin.* 28 (2012) 2122-2128.
- [43] Y. huo, Y. jin, J. zhu, H. li, *Appl. Catal. B: Environ.* 89 (2009) 543-550.
- [44] S. Riyapan, Y. Boonyongmaneerat, O. Mekasuwandumrong, H. Yoshida, S.-I. Fujita, M. Arai, J. Panpranot, *J. Mol. Catal. A: Chem.* 383-384 (2014) 182-187.
- [45] N.S. Babu, N. Lingaiah, N. Pasha, J.V. Kumar, P.S.S. Prasad, *Catal. Today* 141 (2009) 120-124.
- [46] N. Iwasa, T. Mayanagi, W. Nomura, M. Arai, N. Takezawa, *Appl. Catal. A* 248 (2003) 153-160.
- [47] J. Xu, K. Sun, L. Zhang, Y. Ren, X. Xu, *Catal. Commun.* 6 (2005) 462-465.
- [48] R. Zanella, V. Rodríguez-González, Y. Arzola, A. Moreno-Rodríguez, *ACS Catalysis* 2 (2012) 1-11.
- [49] J.A. Wang, A. Cuan, J. Salmones, N. Nava, S. Castillo, M. Morán-Pineda, F. Rojas, *Appl. Surf. Sci.* 230 (2004) 94-105.
- [50] A.I. Osman, J.K. Abu-Dahrieh, F. Laffir, T. Curtin, J.M. Thompson, D.W. Rooney, *Appl. Catal. B: Environ.* 187 (2016) 408-418.
- [51] M.-S. Kim, S.-H. Chung, C.-J. Yoo, M.S. Lee, I.-H. Cho, D.-W. Lee, K.-Y. Lee, *Appl. Catal. B: Environ.* 142-143 (2013) 354-361.
- [52] M. Hosseini, S. Siffert, H.L. Tidahy, R. Cousin, J.F. Lamonier, A. Aboukais, A. Vantomme, M. Roussel, B.L. Su, *Catal. Today* 122 (2007) 391-396.
- [53] A.A. Murashkina, P.D. Murzin, A.V. Rudakova, V.K. Ryabchuk, A.V. Emeline, D.W. Bahnemann, *J Phys Chem C* 119 (2015) 24695-24703.
- [54] W. Zhang, X. Pei, J. Chen, H. He, *Mater. Sci. Semicond. Process.* 38 (2015) 24-30.
- [55] G. Mohan Kumar, P. Ilanchezhiyan, A. Madhan Kumar, S.U. Yuldashev, T.W. Kang, *Chem. Phys.*

- Lett. 649 (2016) 130-134.
- [56] D.M. de los Santos, T. Aguilar, A. Sanchez-Coronilla, J. Navas, N. Cruz Hernandez, R. Alcantara, C. Fernandez-Lorenzo, J. Martin-Calleja, *Chemphyschem* 15 (2014) 2267-2280.
- [57] Q. Zhang, T. Gao, J.M. Andino, Y. Li, *Appl. Catal. B: Environ.* 123-124 (2012) 257-264.
- [58] L. Schlur, S. Begin-Colin, P. Gilliot, M. Gallart, G. Carre, S. Zafeiratos, N. Keller, V. Keller, P. Andre, J.M. Greneche, B. Hezard, M.H. Desmots, G. Pourroy, *Mater. Sci. Eng. C Mater. Biol. Appl.* 38 (2014) 11-19.
- [59] D. Leinen, A. Fernández, J.P. Espinós, J.P. Holgado, A.R. González-Elipe, *Appl. Surf. Sci.* 68 (1993) 453-459.
- [60] O. Hernández-Cristóbal, J. Arenas-Alatorre, G. Díaz, D. Bahena, M. J. Yacamán, *J Phys Chem C* 119 (2015) 11672-11678.
- [61] A.S. Mamede, G. Leclercq, E. Payen, P. Granger, L. Gengembre, J. Grimblot, *Surf. Interface Anal.* 34 (2002) 105-111.
- [62] V.V. Kaichev, M. Morkel, H. Unterhalt, I.P. Prosvirin, V.I. Bukhtiyarov, G. Rupprechter, H.J. Freund, *Surf. Sci.* 566-568 (2004) 1024-1029.
- [63] Y. Bi, G. Lu, *Appl. Catal. B: Environ.* 41 (2003) 279-286.
- [64] J.C. Colmenares, A. Magdziarz, M.A. Aramendia, A. Marinas, J.M. Marinas, F.J. Urbano, J.A. Navio, *Catal. Commun.* 16 (2011) 1-6.
- [65] M. Aramendia, J. Colmenares, A. Marinas, J. Marinas, J. Moreno, J. Navio, F. Urbano, *Catal. Today* 128 (2007) 235-244.
- [66] H. Huang, D.Y.C. Leung, *ACS Catalysis* 1 (2011) 348-354.
- [67] H. Zhang, H. Yan, N. Mao, *Ind. Eng. Chem. Res.* 53 (2014) 2030-2041.
- [68] P. Pichat, J.M. Herrmann, J. Disdier, M.N. Mozzanega, H. Courbon, *Secondary Journal* Volume 19 (1984) 319-326.
- [69] L. Ouyang, P.-f. Tian, G.-j. Da, X.-C. Xu, C. Ao, T.-y. Chen, R. Si, J. Xu, Y.-F. Han, *J. Catal.* 321 (2015) 70-80.
- [70] S.K. Pathak, A. Abate, P. Ruckdeschel, B. Roose, K.C. Gödel, Y. Vaynzof, A. Santhala, S.-I. Watanabe, D.J. Hollman, N. Noel, A. Sepe, U. Wiesner, R. Friend, H.J. Snaith, U. Steiner, *Adv. Funct. Mater.* 24 (2014) 6046-6055.
- [71] A. Tarafdar, S. Biswas, N.K. Pramanik, P. Pramanik, *Micropor. Mesopor. Mater.* 89 (2006)

204-208.

Highlights:

- Palladium catalysts supported on Al-doped TiO₂ mesoporous materials were studied
- The introduction of aluminium can enhance TiO₂ anatase thermostability and increase defect TiO₂.
- The Pd/Al-TiO₂ catalysts possess higher ethanol conversion and CO₂ yield compared Pd/TiO₂.
- The influence of aluminium on SMSI and on ethanol oxidation of catalytic performance of Pd/TiO₂ catalysts were evaluated by TPR and XPS.

